Oxidation of Metals, Vol. 63, Nos. 5/6, June 2005 (© 2005)
DOI: 10.1007/s11085-005-4392-3

Oxidation Mechanism of Steels in Liquid–Lead Alloys

J. Zhang*‡ and N. Li†

Received September 30, 2004; revised January 26, 2005

The oxidation mechanism of steels in liquid–lead alloys (lead or lead–bismuth) was studied. Parametric dependencies of oxidation, including oxygen-concentration effects, oxidation-rate constant and corrosion-rate effects, are analyzed. An oxidation model is developed based on the assumptions that the chemical reactions are at equilibrium locally, and scale removal is due to mass-transfer corrosion. The model shows that outward-iron diffusion in the solid phase (oxide layer) controls the oxide growth and mass-transfer rate in the flowing-boundary layer determines the corrosion-product transport in the liquid phase (liquid–lead alloy). The oxide thickness depends on both the parabolic oxide-growth-rate constant and the mass-transfer-corrosion rate. For long-term operation, the outer layer of a duplex-oxide layer can be completely removed by flowing lead alloys and it is expected that a pure-chromium-oxide layer forms underneath the Fe–Cr spinel if iron is heavily depleted. The oxide thickness and steel weight change are very different from those of the pure parabolic law and they are classified into distinct and universal categories. The model is validated partially by application to interpreting the measured oxide behavior of several steels in a lead-bismuth eutectic-test loop.

KEY WORDS: corrosion; oxidation; liquid metal; oxide layer.

*Decision and Application Division, Los Alamos National Laboratory, Los Alamos, NM 87545, USA.
†Materials Science and Technology Division, Los Alamos National Laboratory, Los Alamos, NM 87545, USA.
‡To whom correspondence should be sent; Tel.: +1-505-667-7444; fax: +1-505-665-2897; Email: jszhang@lanl.gov

INTRODUCTION

Corrosion of containment and structural materials presents a critical challenge in the use of lead–bismuth eutectic (LBE) or liquid lead as a nuclear coolant in accelerator-driven systems (ADS) and advanced reactors. The corrosion in lead-alloy systems is primarily due to the relatively high solubility of the base and major alloying components of steels, such as Fe, Ni, Cr, etc.[1] The process depends on many factors including the flow velocity, temperature and its profile, compositions of the liquid and solid materials.[2] Without some protective means, the selective dissolution of materials would destroy the containment structure rapidly. Efforts have been devoted to finding ways to form and keep protective films on structural metals to reduce corrosion. It was reportedly achieved in Russia.[3] through the application of an active-oxygen-control technique. By carefully controlling the oxygen concentration in LBE or liquid lead, it is possible to maintain an iron and chromium oxide-based layer on the steel surfaces, while keeping lead and bismuth from contamination by excessive oxidation. The oxide film effectively separates the steels from the liquid metal, and therefore the corrosion rate is significantly reduced. The active-oxygen control allows maintenance and restoration of protective-oxide films.[4]

The oxide layer formed on steel surfaces in liquid–lead alloy systems serves as an effective solid-state diffusion barrier between the steel and the liquid–lead alloys. The ideal protective-oxide layer should be pore-free, crack-free, stress-free at operating temperatures, resistant to spalling and damage during cooling or heating.[5] In addition, the oxygen and metal ions must have low diffusion coefficients through the scale, and the recession rate of the original surface must be low enough during the desired service life.[6] For a practical lead-alloy-coolant system, it is nearly impossible to set up such an ideal protective layer. However, it is possible to optimize the self-healing layer by controlling the oxygen concentration in the liquid lead/lead-bismuth, and changing steel compositions and operating conditions.

To optimize the protective layer in lead-alloy-coolant systems, experiments are being conducted in many countries.[7–17] Several important conclusions can be drawn from previous experiments.[18] However, the results are still scarce and scattered and we cannot reach definitive conclusions or correlations between corrosion/oxidation and hydraulic factors, oxygen concentration, and steel composition based on the available data. At the present time, these test results cannot be easily interpreted and applied for general design purposes. It is very difficult to forecast long-term corrosion of steels in liquid-lead alloys based on the experimental results of similar steels that have similar chemical compositions.

Therefore, it is important to develop theoretical tools to interpret the existing data and apply them to practical designs of lead-alloy-coolant systems. In addition, theoretical analysis can guide future experiments. In the present study, a model for the oxidation of steels in lead-alloy environments is developed. The model is based on Wagner's theory,[19] and the mass-transfer corrosion due to the flowing liquid is included using Tedmon's equation.[20] The model is partially benchmarked by experimental results.

To our best knowledge, there is no such oxidation/corrosion model of steel in flowing liquid lead or lead-bismuth. However, several oxidation models of steel in aqueous environment have been presented.[21] Since steel-alloying components can dissolve into both aqueous media and liquid–lead alloys, it is necessary to briefly review the oxidation model of steels with scale removal in aqueous environments.

Recognizing that the diffusion of oxygen ions in the scale is too slow to account for the inner-layer formation, Castle and Masterson[22] developed a model in which it was assumed that the liquid, water, could reach the substrate surface through the porous oxide layer. Therefore, for a duplex-oxide layer, Castle and Masterson hypothesized that the oxidant reaching the steel surface through pores formed the inner layer, while the dissolved metals at pore bases diffused outwards and precipitated to form the outer layer. Based on Castle and Masterson's assumptions, Winkler *et al.*[23] developed a model in which it was assumed that both the inner and outer layers were formed via the precipitation of the dissolved metal in the liquid. Lister *et al.*[24] proposed that the formation of the outer layer was due to the metal precipitation similar to that in Castle and Masterson's model, while they proposed that the inner layer was formed via the solid diffusion of the oxidant through the scale.

These solution-pores-related models are all based on the mechanism that the outer-layer formation is due to the precipitation of the dissolved metals. However, it is noted that duplex-oxide layers also commonly form during gaseous oxidation of metals/alloys.[25] Experimental results have shown that the outer layers in gas can form on the gas/oxide interface, which indicates that the formation is due to solid diffusion of metal through the scale.[26] To be consistent with gaseous oxidation, Gibbs[27] slightly modified Castle and Masterson's model and proposed that pores were only involved to supply the oxidant to the oxide/steel interface, but the oxidation rate was determined by the solid diffusion of metal through the scale to the oxide/media interface. Voids are always observed in oxide films, but experimental investigations[28] concluded that the voids do not aggregate to pores traversing through the outer-oxide layer. Robertson[25, 29] re-examined the pore-relevant model for aqueous oxidation. He pointed

out that there were three main shortcomings: first, it does not account for the similarity of oxidation rates in steam and neutral water; second, it predicts a temperature dependence of the rate which is an order of magnitude too low; and third, direct measurements of the permeability of the oxide suggest that the effective pore size is too small to account for the observed corrosion rate.

Robertson[25, 29] developed his oxidation model in aqueous environments based on analyzing oxide growth in steam and water at high temperatures. It was assumed that the outer-layer formation (for stainless steels, mainly Fe_3O_4) was due to solid-state diffusion of iron, while the inner layer (mainly Fe–Cr spinel) was due to water reaching the inner surface through micro-pores. The oxidation rate was determined by the diffusion rate through the inner layer where the oxide was compact. Therefore, the total corrosion rate in Robertson's model was independent of the liquid-flow velocity and the presence of any outer layer.

As discussed above, tests of steels in flowing-lead alloys indicate that the oxide-layer thickness depends strongly on the flow velocity and the oxygen dissolved in the liquid. Therefore Robertson's model cannot be applied to the present cases. In this study, a model, involving both oxidation and corrosion of steels in liquid–lead alloys, is developed. The species transport in the solid phase (oxide layer) and the liquid phase (liquid–lead alloy) are discussed and modeled. The amount of metal diffusing outward consists of two parts: one part forms new oxide at the liquid/oxide interface, and the other is removed by the flowing liquid. The scale removal by mass-transfer corrosion leads to a high oxidation rate. Unlike Robertson's model for aqueous media, it is found that there is a limiting-oxide thickness depending on the parabolic oxidation rate and the mass-transfer rate. The oxide thickness is strongly affected the flow velocity, which is consistent with test results of steels in lead–bismuth eutectic (LBE).

IDENTIFICATION OF THE OXIDE STRUCTURE

The oxide-layer structure of steel in liquid–lead alloy with oxygen control, in principle, depends on steel compositions, temperature and hydraulic factors. Generally, there are two possible structures for martensitic steels according to the available experimental results:[30]

(1) For temperatures below 550°C, the scale is composed of an external magnetite layer, Fe_3O_4 and a compact internal Fe–Cr spinel-oxide layer. In some cases, the external-magnetite layer is not observed. Penetrations of lead are sometimes observed in the outer layer. The duplex-layer can protect steels from dissolution.

(2) For temperature above 550°C, an internal-oxidation zone with oxide precipitates along the grain boundaries is observed below the Fe–Cr spinel layer.

Austenitic steels have more Cr and Ni than martensitic steels. The oxide layer formed on austenitic steels has the following possible structures:[18]

(1) For temperature below 500°C, the oxide layer is very thin and is composed of the single-layer Fe–Cr spinel, which can prevent direct dissolution.
(2) For temperature around 550°C, the oxide layer can have either duplex- or single-layer structure, depending on the surface and operating conditions. The duplex-layer oxide can prevent steel-component dissolution, while heavy dissolution is observed when the single-layer oxide forms.
(3) For temperature above 550°C, heavy dissolution occurs.

For a static test case, if the liquid is saturated with the steel components, no steel components can be released to the solution. The oxide structures are similar to that in gaseous environment. For other cases with scale removal, the possible oxide structures of stainless steels (martensitic or austenitic steels) in liquid–lead alloys with oxygen control are shown in Fig. 1.

Initially, a very thin oxide layer forms on the steel surface quickly if a steel is exposed to oxidizing environments without protection. After

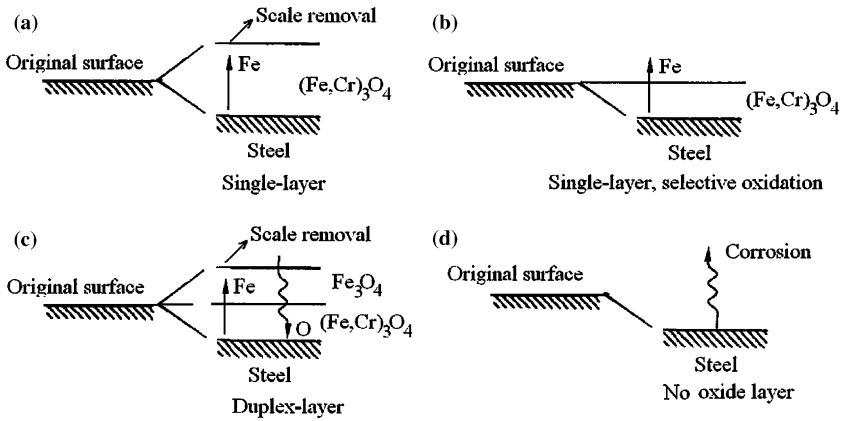

Fig. 1. Possible oxide structures of stainless steels in liquid–lead alloys with oxygen control.

the thickness reaches 2–3 nm[29], the oxidation slows down and the metal or the oxidant diffusion controls the oxidation process. In liquid–lead alloy systems, the flowing solution (lead-alloys) can remove metals at the outer surface. If the removal rate is greater than the diffusion rate of metal through the scale, no new oxide can form at the outer surface (liquid/oxide interface), and the oxide may be formed at the oxide/steel interface. For Fe–Cr steels, the Fe–Cr spinel initially formed can retain Cr and other components such as Ni at their original locations because they have smaller diffusion rates through the scale than that of Fe.[29] Fe diffuses outwards and is carried away at the liquid/oxide interface by the flowing liquid (Fig. 1b). The new oxide formed at the oxide/steel interface takes up the space left by Fe diffusion. Such selective-oxide layer growth is controlled by Fe diffusion.

With increasing operation temperature and Fe content in the steel, the amount of Fe reaching the liquid/oxide interface increases. When it is larger than the amount of Fe removed by the flowing liquid, the excess Fe will be oxidized and new oxide layer forms at the liquid/oxide interface. Thus a duplex-oxide layer forms on the steel surface (Fig. 1c). According to the experimental results from gaseous environments, it appears that the inner-/outer-oxide layer interface coincides with the original-steel surface.

It is noted that the mechanism of duplex-oxide-films formation is very complicated and not well understood at the present even in gaseous environments. In a very simple manner, it can be depicted as:[17] Fe diffuses outwards through each of the oxide layers and produces a pure iron-oxide layer at the liquid/oxide interface. The limited Cr-diffusion leads to Cr-enrichment in the spinel layer near the oxide/alloy interface. Simultaneously, oxygen goes inwards through the outer oxide layer and produces an inner spinel-oxide layer. Since the oxygen self-diffusion coefficient is very small, there should be some fast paths for oxygen to arrive at the inner layer at sufficiently high rates to account for the observed inner-oxide growth.

If the oxygen concentration is too low to form the protective-oxide layer, heavy dissolution or corrosion occurs (Fig. 1d) since most of the steel components have high solubility in liquid–lead-alloys.[18] Such corrosion can also occur at high temperatures[9] if the oxide layer cannot prevent steel components from dissolving. It is important to point out that the oxide-layer structure strongly depends on the steel composition, such as contents of Cr and Si. Discussions on the effects of Cr content can be found in Ref. 29 for aqueous environments, and that of Si content can be found in Ref. 31 for gaseous environments.

THEORY

Wagner Theory for Oxide Growth

After a short "transient" time (the initial-oxidation period), the oxidation rate is controlled by mass (oxygen or metal) diffusion. For such a steady-state situation, the well-known Wagner theory[19, 32, 33] can be used to analyze the oxide growth. In this theory, it is assumed that local thermodynamic equilibrium is attained, while the whole system is not in equilibrium and each component can be assigned a chemical potential which is a function of the position normal to the steel surface.[31] The metal flux J_M through the oxide, which is also a function of position, can be expressed as:

$$J_M = -\frac{D_{M,s} c_M}{RT} \frac{d\mu_M}{dx}, \tag{1}$$

where R is the gas constant, T is the absolute temperature, c_M is the local concentration of metal in the oxide, and $D_{M,s}$ is the metal self-diffusion coefficient. The relation between the self-diffusion coefficient and the chemical diffusion coefficient $D_{M,c}$ (Fick's law) is:

$$D_{M,c} = \frac{D_{M,s}}{RT} \frac{d\mu_M}{d \ln c_M}, \tag{2}$$

In Eqs. 1 and 2, μ_M is the chemical potential of the metal ion. It can be expressed in term of chemical potential of oxygen by:[34]

$$\mu_M = -\alpha \mu_o = -\frac{\alpha}{2} RT \ln P_{O_2}, \tag{3}$$

where μ_O is the oxygen-atom chemical potential and P_{O_2} is the oxygen partial pressure, and α is the ratio of the mole fraction of oxygen in the oxide to that of the metal, for example $\alpha = 4/3$ for Fe_3O_4. Substituting Eq. 3 into Eq. 1:

$$J_M = \frac{1}{2} \alpha D_{M,s} c_M \frac{d \ln P_{O_2}}{dx}. \tag{4}$$

It has been found that most of the growth of the thick films ($> 1\,\mu m$) follows parabolic kinetics, i.e.,

$$X^2 = K_p t, \tag{5a}$$

or

$$\frac{dX}{dt} = \frac{K_p}{2X}, \tag{5b}$$

where t is time, X is the oxide layer thickness at time t, and K_p is the parabolic-growth-rate constant depending on the operating conditions. Based on Eqs. 4 and 5 and following Wagner's procedure, it was found:[32]

$$K_p = \int_{(P_{O_2})_I}^{(P_{O_2})_{II}} \alpha D_{M,s} d \ln P_{O_2}, \tag{6}$$

where the subscript I and II represent the oxide/steel and oxide/environment boundary. Taking into account the effects of oxygen diffusion and correlating the constant to the tracer-diffusion coefficient, $D_{i,t}(i = O, Fe)$, which is readily obtained experimentally, it was found:[26]

$$K_p = \int_{(P_{O_2})_I}^{(P_{O_2})_{II}} \left(\frac{\alpha D_{M,t}}{f_M} + \frac{D_{O,t}}{f_O} \right) d \ln P_{O_2}. \tag{7}$$

In the above expression, f_M (of metal M) and f_O (of oxygen) are coordinate factors for the self-diffusion mechanism and are of the order unity. For Fe_3O_4, the value of f_{Fe} is approximately 0.5 for a mechanism involving vacancy and in the range 0.4–1 for a mechanism involving interstitials.[35] Taking into account that the oxygen-tracer diffusion in an oxide layer is much smaller than that of iron, i.e. $D_O << D_M$, most oxidation processes are controlled by the outward diffusion of metal ions. Thus the second term in the integration (Eq. 7) can be neglected and the expression reduces to Eq. 6.

If the oxide formation is controlled by lattice and short-circuit diffusion (diffusion along grain boundaries), the tracer-diffusion coefficient in Eq. 7 should be replaced by an effective-diffusion coefficient that is defined as:[36]

$$D_{\text{eff}} = D_L(1 - \Phi) + D_B \Phi, \tag{8}$$

where D_{L} and D_{B} are the lattice-diffusion coefficient and the diffusion coefficient along grain boundaries respectively, Φ is the fraction of the diffusion sites related to short-circuit paths. Assuming that the oxide grains are small rectangular prisms with width and length g, height ε, the fraction can be expressed as:[37]

$$\Phi = \frac{2\varepsilon}{g}, \tag{9}$$

Equation 7 and the related equations are very important in the oxide-growth theory. It provides a quantitative relationship between the parabolic oxidation rate constant with the self-diffusion coefficients of

metal ions that are easily obtained experimentally. Evaluation of the oxidation rate constant from Eq. 7 merely requires that data available for the tracer diffusion coefficient that depends on the oxygen partial pressure, making it possible to forecast long-term oxidation behavior based on short-term experiments and to guide future experiments.

Point-defect Theory for Cation Diffusion in Oxide Layers

It has been noted that the diffusion rate of oxygen in magnetite and Fe–Cr spinel is much smaller than that of iron ions. It is the outward diffusion of iron that controls oxide growth in liquid–lead alloys. For solid-state diffusion, the concentration of point defects (vacancies-and interstitials) determines the diffusion rate. Experimental results of diffusion of Fe in Fe_3O_4[38] are shown in Fig. 2, as well as the fitting results. The figure shows that the tracer-diffusion coefficient depends strongly on both oxygen partial pressure and temperature. There is a minimum value for the coefficient at each temperature. The phenomenon can be explained using the point-defect theory:[39] at low-oxygen pressure, the Fe diffusion is determined by the movement of Fe interstitials which decreases with increasing oxygen partial pressure, while at high-oxygen pressures, the diffusion is controlled by vacancies.

Theoretical analyses of iron diffusion in magnetite have been studied in detail.[39–41] For our purpose, we will derive the dependency of the diffusion coefficient on the oxygen pressure and temperature in liquid–lead alloys. Similar to the gaseous oxidation, Fe vacancies (V_{Fe}^{2-}) are produced via:

$$\frac{4}{3}O = \frac{1}{3}Fe_3O_4 + V_{Fe}^{2-} + 2h^+, \tag{10}$$

where h^+ is a hole. The equilibrium constant of the above reaction, K_{10}, is:

$$K_{10} = \frac{(a_{Fe_3O_4})^{1/3} a_{V_{Fe}^{2-}} (a_{h^+})^2}{a_O^{4/3}} = \frac{c_{V_{Fe}^{2-}} (c_{h^+})^2}{(P_{O_2})^{2/3}}, \tag{11}$$

where a is the activity. Therefore

$$c_{V_{Fe}^{2-}} = \frac{K_{10}(P_{O_2})^{2/3}}{(c_{h^+})^2} \propto (P_{O_2})^{2/3}. \tag{12}$$

For Frenkel Defects,[42] the Fe interstitial, Fe_I^{2+}, is produced via:

$$Fe_{Fe} = Fe_I^{2+} + V_{Fe}^{2-}, \tag{13}$$

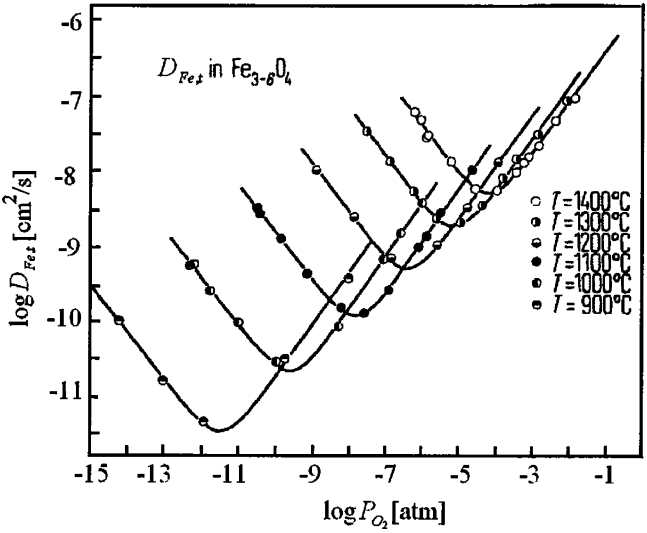

Fig. 2. Iron-tracer-diffusion coefficient in magnetite as a function of the oxygen partial pressure in the temperature range of 900 to 1400°C.[38]

then, the interstitial concentration $c_{\mathrm{Fe}_\mathrm{I}^{2+}}$ can be expressed in terms of the equilibrium constant K_{13} of the above reaction and the vacancy concentration as:

$$c_{\mathrm{Fe}_\mathrm{I}^{2+}} = \frac{K_{13}}{c_{V_{\mathrm{Fe}}^{2-}}} \propto (P_{O_2})^{-2/3}. \tag{14}$$

The self-diffusion coefficient of iron in Fe_3O_4 involving defects can be written as:[43]

$$D_{Fe,s} = \sum_{def} D_{def} c_{def}, \tag{15}$$

the subscript def represents defects. The tracer-diffusion coefficient in Eq. 7 can be expressed as:

$$\begin{aligned} D_{Fe,t} &= f_{Fe} D_{Fe,s} = D_V^0 \exp(-E_V/RT) P_{O_2}^{-2/3} \\ &\quad + D_\mathrm{I}^0 \exp(-E_I/RT) P_{O_2}^{-2/3}, \end{aligned} \tag{16}$$

where D_V^0 and D_I^0 are constants related to vacancies and interstitials and they both have the unit of a diffusion coefficient. E_V and E_I are

apparent-activation energy. It has been found that Eq. 17 could also be applicable to the tracer diffusion of iron in spinel $(Fe,Cr)_3O_4$.[43] For the Fe-tracer-diffusion coefficient in magnetite, in the temperature range of 900 to 1400°C, Dieckmann and Schmalzried[38] found:

$$D_V^0 = 4 \times 10^{-15}\,\mathrm{m^2/s}, \quad D_I^0 = 8 \times 10^3\,\mathrm{m^2/s},$$
$$E_V^0 = -138.6\ \mathrm{kJ/mol}, \quad E_I^0 = -614.2\ \mathrm{kJ/mol}. \tag{17}$$

Comparison between the calculation based on Eq. 17 using the values provided in Ref. 38 and experimental results at 500°C[44] indicates that the values for the constants in Eq. 17 taken from Ref. [38] is also valid at 500°C. To the best of our knowledge, there is no temperature-dependence expression for the Fe-tracer-diffusion coefficient in Fe–Cr spinel. Topfer, *et al.*[43] studied the diffusion coefficient in detail at 1200°C. Comparisons of Fe-and Cr-tracer-diffusion coefficient in Fe–Cr spinel for different Cr content are shown in Fig. 3. At temperature 1200°C, the Fe-tracer-diffusion coefficient decreases with increasing Cr content in the spinel. The Cr-tracer-diffusion coefficient is much smaller than that of Fe at the same temperature, therefore during the oxidation process Cr remains at the original locations, while Fe diffuses through the scale to form new oxides. Studies of metal diffusion in the spinel indicate that the diffusion coefficients can be ranked as Mn > Fe > Co > Ni > Cr.[25]

Mass Transport of Corrosion Products in the Liquid Metal

Different from oxidation processes in gaseous environments, steel components can be dissolved into liquid lead or lead–bismuth because the main components such as Fe, Ni, Cr have high solubility in the liquid-metal alloy. Two processes (dissolution and oxidation) occur simultaneously at the steel surface in contact with the liquid lead/LBE with oxygen control. The flowing liquid carries away the dissolved metals (corrosion products), which sustains corrosion. For mass-transfer corrosion, the corrosion product concentration in the liquid satisfies (ignoring chemical reactions in liquid due to low concentrations):

$$\frac{\partial c_i}{\partial t} + \mathrm{U}\nabla c_i = D_i \nabla^2 c_i, \tag{18}$$

where c_i is the concentration of corrosion product i in wppm, D_i is the diffusion coefficient of corrosion product i in the liquid, and U is the velocity vector. At the liquid/steel interface, the corrosion product concentration is at equilibrium. For the case without the oxide layer:[4]

$$c_{i,w} = c_{i,s} = 10^{A_i + B_i/T}, \tag{19a}$$

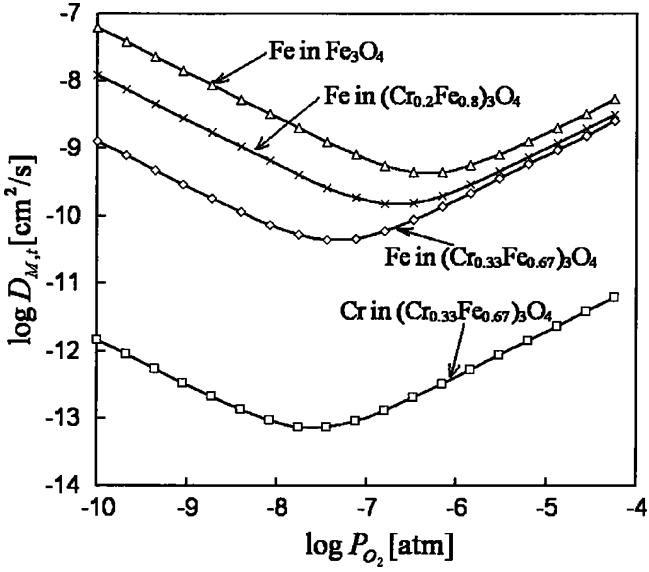

Fig. 3. Fitted results of Fe-and Cr-tracer-diffusion coefficient in $(Cr_{1-x}Fe_x)_3O_4$. The fitted equation for $x = 0$ is taken from Ref. 38, and the other equations are taken form Ref. 43.

and for the case with the oxide layer:[18]

$$c_{i,w} = c_{i,s} a_{pb}^{b/a} \left(\frac{c_{O,s}}{c_O} \right)^{b/a} \exp\left[\frac{1}{aRT} (\Delta F_{M_a O_b} - b\Delta F_{PbO}) \right], \qquad (19b)$$

where $c_{i,w}$ is the boundary concentration (concentration at the interface), $c_{i,s}$ is the solubility of metal i in the liquid (liquid lead or LBE), a_{Pb} is activity of lead,[18] ΔF is the free Gibbs energy of formation for the oxide, a and b are stoichiometric constants of oxide $M_a O_b$.

Knowing the corrosion-product concentration at the interface, the corrosion flux, q_i, can be calculated using Fick's law:

$$q_i = -D_i \frac{dc_i}{dy}|_{y=0} \approx K_{i,m}(c_{i,w} - c_{i,b}), \qquad (20)$$

where $K_{i,m}$ is the mass-transfer coefficient, depending on the local hydraulic factors such as the streamwise mean velocity, hydraulic diameters and local temperature. $c_{i,b}$ is the concentration of corrosion product i in the bulk flow and is often set to $c_{i,b} = 0$. For a non-isothermal, closed-loop system, the bulk concentration can be calculated by taking into account that the total amount of corrosion equals the total amount of precipitation in the entire closed loop.[45]

An analytical solution for the corrosion flux in a non-isothermal liquid lead or LBE loop was obtained as:[46]

$$q_i(x) = \left(\frac{2\pi D_i^2 \gamma}{3L}\right)^{1/3} \frac{1}{Ai(0)\Gamma(1/3)} \sum_k Q_k \exp(2\pi k I x/L), \tag{21}$$

where Ai and Γ are Airy Function and Gamma Function, respectively, γ is the wall shear rate defined by $\gamma = \lambda V^2/2\upsilon$ (γ is the friction factor, V (m/s) is the bulk velocity, υ (m^2/s) is the kinematic viscosity), and $Q_0 = 0$, $Q_k = a_k k^{1/3} I^{1/3}$ for $k > 0$ and $Q_k = a_k |k|^{1/3}(-I)^{1/3}$ for $k < 0$. I is the imaginary unit, and it is chosen that $I^{1/3} = \sqrt{3}/2 + I/2$ and $(-I)^{-1/3} = \sqrt{3}/2 - I/2$.

To calculate the corrosion rate of steel in liquid–lead-alloy environments, it is necessary to evaluate the value of the diffusion coefficient of corrosion products (Fe, Cr, Ni, etc). A correlation of the Fe-diffusion coefficient in pure liquid lead was developed by Robertson:[47]

$$D_{Fe\rightarrow Pb} = 4.9 \times 10^{-7} \exp\left(-\frac{44100 \pm 6300}{RT}\right) \mathrm{m}^2/\mathrm{s}. \tag{22}$$

To our best knowledge, there is no correlation for Fe diffusion in LBE. By comparing the two diffusion coefficients (Fe in pure liquid lead and in LBE) at 750°C, Balbaud-Celerier and Barbier[47] found that the two values are almost the same. Therefore, they assumed the Fe-diffusion coefficient in LBE equals to that in pure lead over a considerable temperature range.

Tedmon's Model for Oxidation of Steel in Liquid–lead Alloy with Scale Removal by Mass-Transfer Corrosion

The oxide-layer growth, the corrosion-product transport in the scale and the liquid are discussed in the previous sections. It is necessary to combine all the processes for a complete picture of the oxidation and corrosion behavior of steel exposed to lead-alloys with oxygen control. Tedmon's model,[20] based on the experiments of Cr oxidation at high temperature with scale vaporization, can be applied to the present oxidation process by replacing the vaporization rate with the mass-transfer-corrosion rate. Tedmon's model is:

$$\frac{d\delta}{dt} = \frac{K_p}{2\delta} - K_r, \tag{23}$$

where δ is the oxide thickness at time t, K_p is the parabolic-oxide-growth-rate constant and is calculated by Eq. 7, K_r is the scale-removal-rate constant

by mass-transfer corrosion and is related to the corrosion flux by:

$$K_r = q\frac{\rho_L}{\rho_{ox}(1-F_O)}, \tag{24}$$

ρ_L and ρ_{ox} are the density of the liquid and the oxide, respectively, and F_o is the mass fraction of oxygen in the oxide. For the zero-oxide-thickness initial condition (no pre-oxidation), the solution of Eq. 23 is:[20]

$$t = -\frac{\delta}{K_r} - \frac{K_p}{2K_r^2}\ln\left|1-\frac{2K_r}{K_p}\delta\right|. \tag{25}$$

For non-zero initial condition, $\delta_0(\delta_0 \neq 0$, pre-oxidation), the solution becomes:[48]

$$t = -\frac{\delta-\delta_0}{K_r} - \frac{K_p}{2K_r^2}\left[\ln\left|1-\frac{2K_r}{K_p}\delta\right| - \ln\left|1-\frac{2K_r}{K_p}\delta_0\right|\right]. \tag{26}$$

Based on Eqs. 25 and 26, the initial and asymptotic kinetics were discussed in Ref. [48]. Several approximate solutions were obtained for the initial and asymptotic behaviors of the oxide growth. Eqs. 25 and 26 indicate that the oxide thickness approaches a limiting thickness $\delta_c(\delta_c = K_p/2K_r)$ for long-term operations ($t \to \infty$) if δ_c is smaller than the limit above which spallation occurs. Such a phenomenon is very different from that of oxidation without scale removal, for which the oxide thickness grows in time until it reaches the spallation thickness.

Typical behavior of oxide thickness for oxidation process with scale removal is shown in Fig. 4. For comparison, the parabolic law result is also shown in the figure. If $\delta_0 > \delta_c$, the thickness approaches δ_c from above, corresponding to oxide dissociation; if $\delta_0 < \delta_c$, the thickness approaches δ_c from below, corresponding to new-oxide formation; if $\delta_0 = \delta_c$, the thickness stays constant in time, indicating that the metal-removal rate by mass-transfer corrosion equals the diffusion rate of cations through the existing oxide layer.

The weight changes of samples are related to the oxide thickness (assuming that the oxide is compact) by:[48]

$$\Delta w = \rho_{ox}F_O x_f(X-X_0) - \rho_{ox}(1-F_O)K_r t. \tag{27}$$

A detailed discussion on the mass changes of samples in high-temperature oxidation in a scale-removal environment can be found in Ref. 48. The typical weight-change curves for steel samples in a liquid–lead-alloy system are shown in Fig. 5. For the parabolic law (corresponding to the liquid being saturated with the corrosion product), the mass always increases with time; for the cases of $\delta_0 < F_O\delta_c$, the weight first increases with time

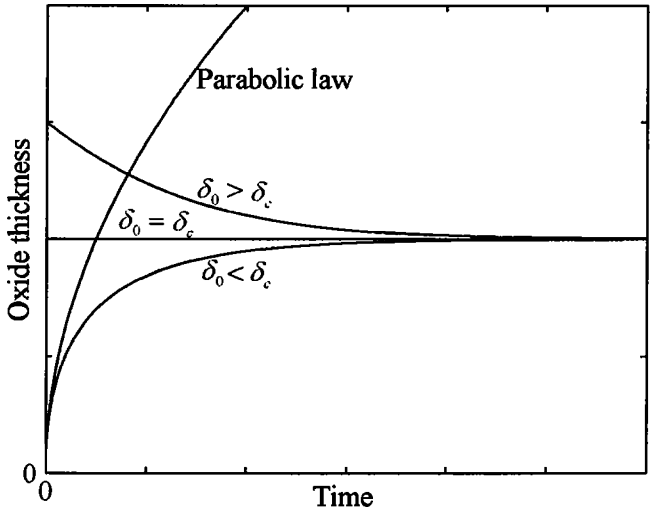

Fig. 4. Typical oxide-thickness variations with time for oxidation with scale removal.

and then decreases after it reaches a maximum; for the cases of $\delta_0 < F_O \delta_c$, the weight always decreases in time. When $K_r \to 0$, Eq. 23 is reduced to the parabolic law, the weight always increases if there is no oxide spallation. This corresponds to most of the static-test cases, and shows that long-term corrosion rates cannot be reliably extracted from static tests.

DISCUSSION

Parametric Dependencies

To avoid lead-oxide precipitation and sustain Fe-oxide (mainly Fe_3O_4) formation, the oxygen partial pressure in the cover gas of a lead-alloy system should be controlled in the range:[18]

$$1/2\Delta F_{Fe_3O_4} < RT \ln P_{O_2} < 2\Delta F_{PbO} - 2RT \ln a_{Pb}. \tag{28}$$

From Eq. 17, the partial pressure for the minimal tracer-diffusion coefficient can be found as:

$$P_{O_2}^{4/3}(D_{Fe,t}^{\min}) = \frac{D_I^0}{D_V^0} \exp\left(-\frac{E_I - E_V}{RT}\right). \tag{29}$$

The maximal and minimal oxygen-partial pressures in a lead-alloy system (lead and LBE) with oxygen controlled and $P_{O_2}(D_{Fe,t}^{\min})$ as func-

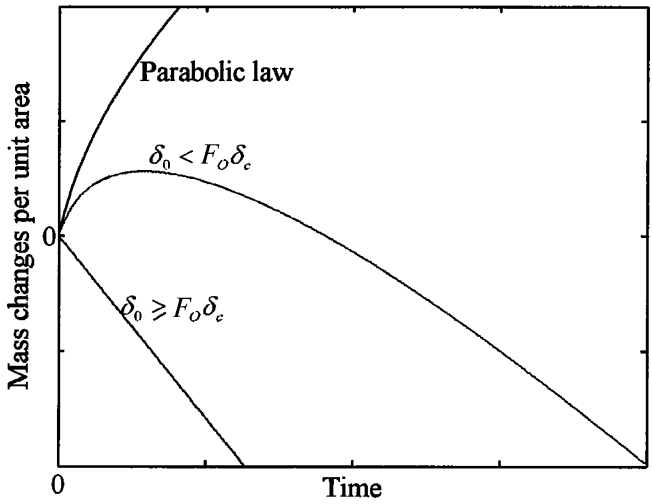

Fig. 5. Typical curves of weight change per unit area for samples in liquid–lead alloy.

tions of temperature are shown in Fig. 6. The figure shows that the oxygen partial pressure for the tracer-diffusion coefficient of iron in Fe_3O_4 attaining its minimal value is less than the maximal partial pressure in the controlled system, while greater than the minimal partial pressure, indicating that Fe diffusion in the oxide can be controlled by either vacancies or interstitials depending the oxygen level in the liquid–lead alloy. According to Eqs. 6 and 17, the parabolic-growth-rate constant of Fe_3O_4 is:

$$K_p = \frac{2}{f_{\mathrm{Fe}}}\left[D_V^0 \exp(-E_V/RT)(P_{O_2})^{2/3} - D_I^0 \exp(-E_I/RT)(P_{O_2})^{-2/3}\right]\Big|_{(P_{O_2})_I}^{(P_{O_2})_{II}}, \tag{30}$$

In liquid–lead alloy systems with oxygen control, it is convenient to express the oxygen, effects in term of the oxygen concentration in the liquid metal. The relation between the oxygen concentration and the oxygen partial pressure at the liquid/oxide interface can be expressed as:[18]

$$(P_{O_2})_{II} = \left(\frac{c_O}{c_{O,s}}\right)^2 a_{\mathrm{Pb}}^{-2} \exp\left(\frac{2\Delta F_{\mathrm{PbO}}}{RT}\right). \tag{31}$$

Equations 30 and 31 indicate that the parabolic rate constant of magnetite depends on oxygen concentration, oxygen solubility in the liquid, the Pb activity and the Gibbs free energy of formation for PbO. If the oxygen activity in the liquid–lead alloy is defined as: $a_O = c_O/c_{O,s}$, then

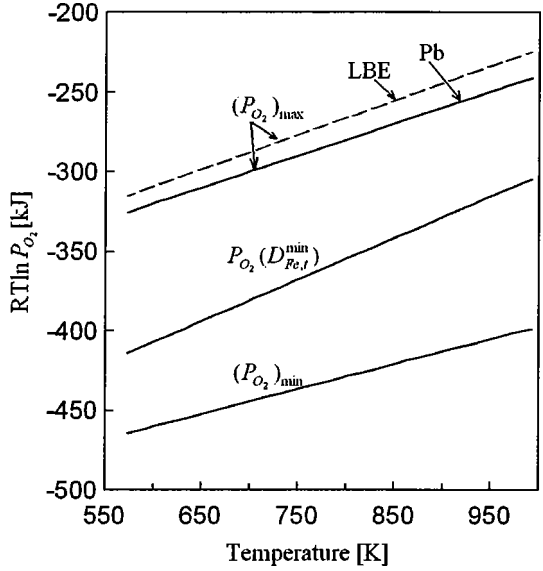

Fig. 6. The oxygen upper-and lower-limits in oxygen-controlled liquid lead and LBE and the oxygen partial pressure for minimal Fe-tracer-diffusion coefficient in magnetite.

$K_p \propto A(a_O)^{4/3} - B(a_O)^{-4/3}$, where A and B are constants depending only on temperature.

For showing the dependencies of K_p on the oxygen concentration in liquid–lead alloy systems, curves of K_p with c_O are shown in Fig. 7 for three typical working temperatures of LBE by assuming that $(P_{O_2})_I$ is the dissociation partial pressure of Fe_3O_4 and setting $f_{Fe} = 0.5$. The figure indicates that K_p increases with c_O when c_O is very small and reaches a constant value for larger c_O. Such phenomena can be explained by taking into account that $a_O \to 1$ with $c_O \to c_{O,s}$, leading to a constant oxygen partial pressure which is the upper limit in Eq. 28 at a given temperature.

For mass-transfer corrosion, the mass-transfer rate, K_m, can be expressed as:

$$K_m = K_m^0 \exp\left(\frac{Q_m}{RT}\right), \tag{32}$$

where K_m^0 depends on the hydraulics factors, such as the flow velocity, liquid viscosity, diffusion coefficient and the hydraulic diameter. Assuming that the bulk concentration of the corrosion product has the same dependence on the oxygen concentration with the surface concentration, based on Eqs. 19b and 24, the scale removal rate, K_r, for Fe_3O_4 can be

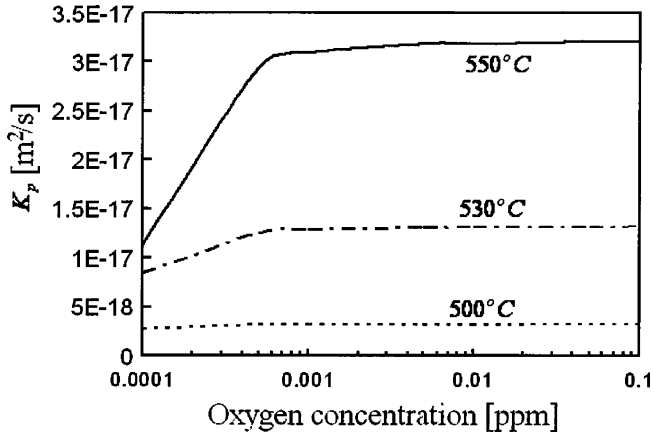

Fig. 7. K_p dependencies on the oxygen concentration in LBE at three typical temperatures.

expressed as:

$$K_r = K_r^0 c_{Fe,s} a_{Pb}^{4/3} \left(\frac{c_{O,s}}{c_O}\right)^{4/3} \exp\left(\frac{Q_r}{RT}\right). \tag{33}$$

Thus, the Fe_3O_4-removal rate depends on the Fe solubility, Pb activity and $\propto (a_O)^{-4/3}$. Eqs. 30 and 33 are used to calculate K_p and K_r. Knowing these two parameters, the limiting-oxide thickness δ_c can be calculated.

The above analyses on Fe_3O_4 growth behaviors in liquid–lead alloys are based on Dieckmann and Schmalzried's theory,[38–40] in which the oxygen dependency is based on the assumption that the defect concentrations (vacancies and interstitials) are independent of the grain size and porosity. In Dieckmann and Schmalzried's experiments, the magnetite had a grain size in the range of 10 to 100 μm. They suggested that the tracer diffusion or the parabolic growth rate constant should be influenced by the oxide physical properties. For fine-grain-magnetite growth, Schmalzried[49] found that the dependency was $(P_{O_2})^{0.4}$ and Surman[50] found that it was $(P_{O_2})^{0.145}$. For the duplex-oxide-layer growth, Smith[51] found the dependency was $(P_{O_2})^{0.135}$ and Saito *et al.*[52] found it was $(P_{O_2})^{0.141}$.

The oxide-layer-formation process is very complex. The existing experimental results in liquid–lead alloy are not enough to produce a correlation between the oxide layer and the oxygen concentration. The parabolic rate constant for the duplex layer of 316 stain steel in CO/CO_2 environment and for SUS 316 steel in a Ni/NiO environment at 600°C are shown in Fig. 8, as well as the constant for magnetite of pure iron in CO/CO_2[50] and gaseous environment.[38] It is difficult to interpret the causes that result

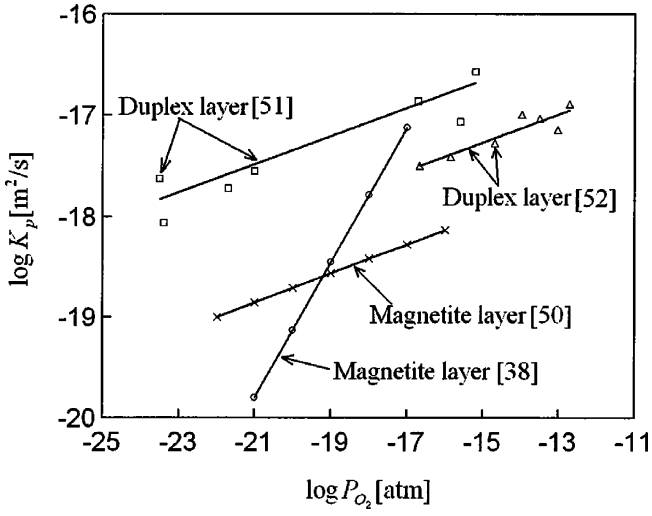

Fig. 8. The parabolic-oxidation rate constant of 316,[51] SUS 316[52] stainless steels and pure iron[38, 49] at 600°C. The constant from Ref. 38 was calculated based on the experimental tracer-diffusion coefficient.

in the difference between the rate constant of the two steels that have the same chemical compositions based on the present theories. It may be due to different oxide gain sizes, the different oxidizing environments, etc. The large different dependence on the oxygen indicates that there are still many open questions in the field of steel oxidation and corrosion.

Rate-control Process

In the present study, it is assumed that the protective layer is continually removed by mass-transfer corrosion. The mass-transfer corrosion does not influence the oxidation mechanism, and the oxidation does not influence the scale-removal mechanism either. The entire process involves surface and bulk reactions, mass transport (diffusion and convection) in the flowing liquid, and species diffusion in the oxide (species diffusion in steel is neglected). The involved processes of duplex-layer formation are shown in Fig. 9.

The chemical reactions are much faster than mass diffusion. Thus it is reasonable to assume that all the chemical reactions are at their local equilibria. In a practical LBE coolant system or an LBE test facility, the flow is fully turbulent and it can mix the corrosion product quickly, then diffusion in the bulk flow is neglected. Compared with mass transport due

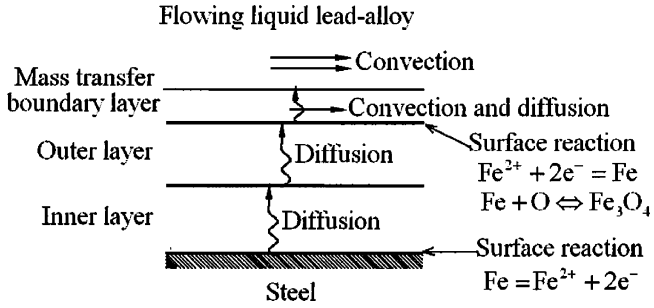

Fig. 9. Iron-transport processes for a duplex-layer.

to diffusion and convection in the boundary layer, the mass transport due to convection in the bulk flow is much faster. Therefore, the mass-transfer rate in the boundary layer dominates the transport in the liquid, while the diffusion process dominates the transport in the oxide. The open question is which process dominates the entire oxide growth with scale removal in a liquid–lead-alloy system with oxygen control.

It has been verified that Cr and Ni have lower diffusion rates in Fe–Cr–Ni spinel than that of Fe[25]. It is commonly accepted that the outward-Fe diffusion determines the entire oxidation rate, Cr and Ni are retained and relatively enriched in the inner layer. The inner layer grows at a rate limited by the space made available by the outward diffusion of Fe ions. Because the Pilling-Bedworth ratios of the oxide are roughly two, about half of the Fe ions move through the scale and the inner-/outer-layer interface coincides with the original steel surface.

In Robertson's[25, 29] model for aqueous oxidation, it was assumed that the corrosion rate was limited by cation diffusion in the inner layer. Such an assumption is reasonable, because the Fe-tracer-diffusion coefficient decreases with increasing Cr content in the Fe–Cr spinel according to Fig. 3. However, the inner-oxide grain size is much finer compared with the outer-oxide grain size, the effective-diffusion coefficient may be larger in the inner layer considering the enhanced diffusion along grain boundaries making diffusion in the outer layer rate determining for the entire corrosion rate. Diffusion of Fe and Cr in the duplex-layer scales grown on 316 stainless steel was studied by Smith[53] in the temperature range 655–1000°C. The results are shown in Fig. 10. The figure indicates that the diffusion coefficient of Fe in magnetite (outer layer) is smaller than that in the Fe–Cr–Ni spinel (inner layer). Smith[53] suggested that the diffusion coefficient was an effective one, and the rate-controlling step of the duplex layer forming on 316 steel could be diffusion in magnetite. The

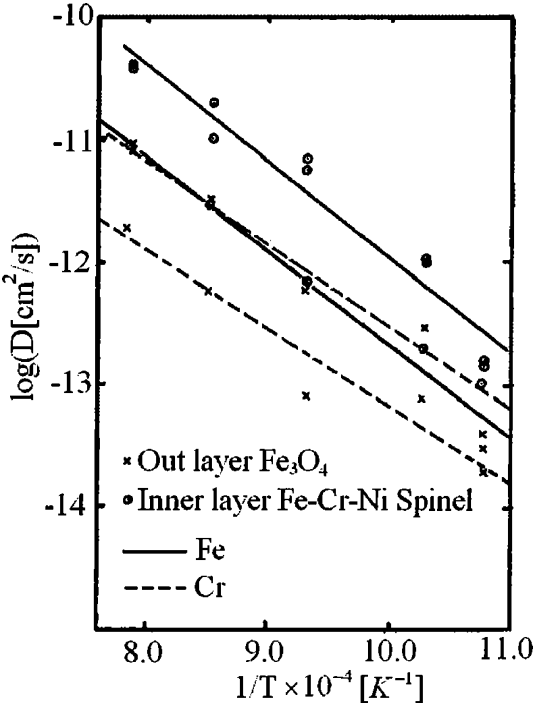

Fig. 10. Curves of Fe, Cr diffusion coefficients in the inner and outer oxide layer as functions of temperature.[53]

same conclusion was also drawn by Daito *et al.*[52], Furuya *et al.*[54] and Smith.[51] Because the diffusion coefficients in magnetite and spinel differ by only one order of magnitude, we can not clearly differentiate which diffusion controls the outward-Fe movement.

The oxide-growth rate is a function of time, while the scale-removal rate by mass-transfer corrosion is constant. If the oxide-growth rate is initially larger than the scale-removal rate, i.e., $K_p/2\delta > K_r$, oxidation dominates the entire corrosion process and the oxide thickness increases with time until it reaches the limiting thickness δ_c. If the oxide-growth rate is initially smaller than the scale-removal rate, i.e., $K_p/2\delta < K_r$; then for pre-oxidation cases, the scale removal dominates the corrosion process and the oxide thickness decreases with time and approaches its limiting thickness from above; for cases of no pre-oxidation, no oxide forms at the liquid/solid interface, and direct dissolution of steel components occurs, and the corrosion rate is determined by the mass-transfer coefficient K_m.

Because the inner layer takes up the space made available by outward-Fe diffusion, it continues to grow even when oxidation and scale removal reach their balance. Therefore, the control-step will eventually be Fe diffusion in the inner-oxide layer. For long-term operations, the amount of Fe diffused through the inner layer cannot balance the amount of removal at the liquid/scale interface. The outer-layer scale (Fe_3O_4) dissociates and is continually removed by the flowing liquid and becomes thinner. Eventually, the Fe_3O_4 scale will be removed completely and the Fe–Cr spinel becomes the layer in contact with the liquid.

On the other hand, it is possible to form Cr_2O_3 scale at the oxide/steel interface because of the depletion of Fe and the low oxygen partial pressure. Once the formation of Cr_2O_3 scale begins, the transport of Fe will be reduced significantly due to its much lower diffusion coefficient in the scale. It is necessary to point out that the corrosion rate or the recession rate of the steel surface with oxide formation is much smaller than that without oxide formation, i.e. direct dissolution, making it possible to use some steels in oxygen-controlled, liquid lead or LBE for extended periods of time.

Erosion Corrosion

The present model assumes that scale removal is due to the mass-transfer corrosion that does not affect the oxidation mechanism. In practice, erosion can occur at the location where the flow changes its direction suddenly, such as a bend, an expansion, etc. The liquid particles can attack the protective layer, and the high shear stress may strip the layer away. Such attacks can enhance the oxidation mechanism and lead to a higher degradation rate of the structure surface.

Chang *et al.*[55] classified the erosion–oxidation phenomena into four categories: erosion of oxide only, erosion-enhanced oxidation, oxidation-affected erosion and erosion of metal only. Rishel *et al.*[56] proposed that there are three types in the erosion-enhanced-oxidation range (Fig. 11). For erosion of the oxide only and type I in the erosion-enhanced-oxidation regime, erosion does not modify the oxidation mechanism. Therefore the present model can be applied by replacing the scale-removal rate of mass-transfer corrosion with that of scale removal by erosion.

For Type II of the erosion-enhanced oxidation, the erosion attack affects the oxidation mechanism and results in fast path for cation diffusion that leads to a higher oxide-growth rate than that without erosion. For such cases, the diffusion coefficient can not be calculated using the point-defect theory, and the fast-path should be considered. Therefore the present model is still valid with some modification of the

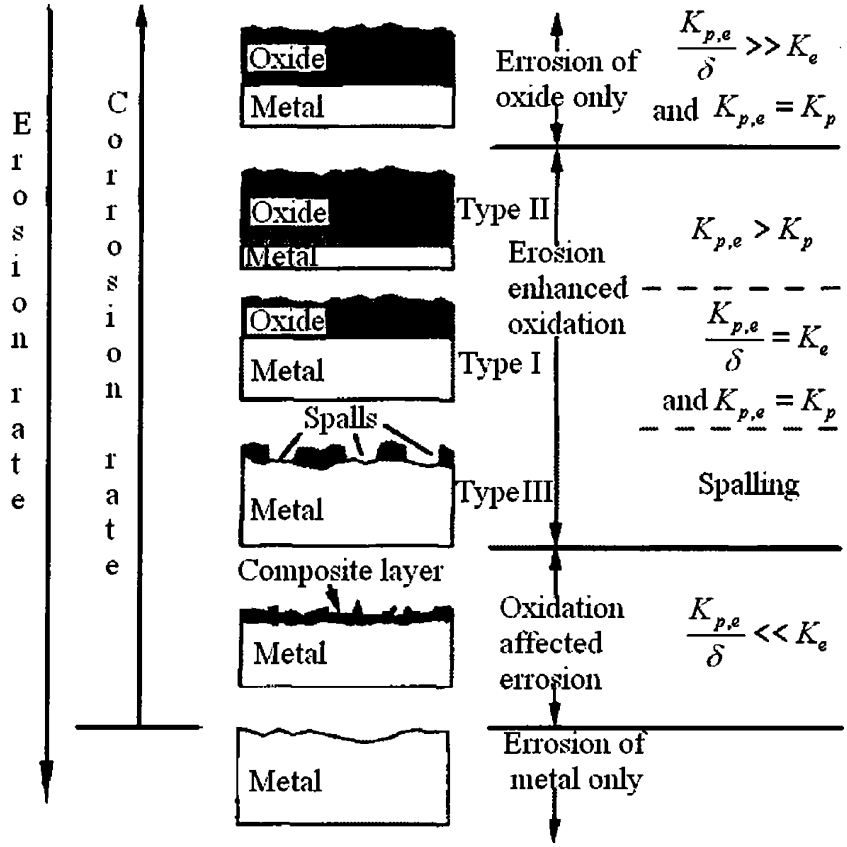

Fig. 11. Erosion-oxidation-interaction regimes.[56] K_e is the erosion rate and $K_{p,e}$ is the parabolic-oxide-growth-rate constant in erosion environment.

diffusion-coefficient calculation. For Type III in which spalling occurs, the Tedmon equation (Eq. 23) cannot be used, because scale removal and the oxide-layer growth are not continuous. Oxide spalling destroys the protective-oxide layer, resulting in new-oxide formation and heavy dissolution, enhancing the corrosion rate significantly. A description of oxide spalling needs a full understanding of the stress within the oxide. Several spalling mechanisms were summarized in Ref. 56.

Oxidation-affected erosion occurs when erosion is rapid compared with oxidation.[55] The oxide layer is thin, discontinuous, and the erosion impacts cause substantial plastic deformation of the underlying steel. For such cases, the substrate is covered with a composite layer composed of

deformed steel, oxidation product and embedded erosion particles.[56] Therefore the present model is no longer applicable in which the covered layer is composed of oxidation product (oxide layer) only. In the absence of the oxide layer, the steel will degrade very rapidly by erosion.

Although erosion and mass-transfer corrosion have some similar features, the parametric dependencies differ significantly because the two processes have completely different mechanisms. To fully understand the erosion effects in lead-alloy-coolant systems, more experimental and modeling studies should be carried out.

APPLICATIONS TO OXIDATION & CORROSION OF STEELS IN PB/LBE

The proposed model is applied to interpret the test results of steel 316, D-9 and HT-9. The experiments were carried out in a LBE loop at 550° C.[17] The LBE flow velocity was 1.9 m/s and the oxygen level is in the range of 0.03–0.05 ppm. Duplex-oxide layer formed after 1000, 2000 and 3000 h exposure. The structures after 2000 h are shown in Fig. 12.

According to Refs. 48 and 57, Eq. 26 can be simplified for early-stage kinetics. The simplified equation is:[57]

$$\delta = (K_p t)^{1/2} - \frac{2}{3} K_r t, \tag{34}$$

Correspondingly, the weight change per-unit can be expressed as:

$$\Delta W = \rho_{Ox} f_O (K_p t)^{1/2} - \rho_{Ox} \left(1 - \frac{1}{3} f_O\right) K_r t, \tag{35}$$

The rate constants (K_p, K_r) can be calculated using the equations proposed in section Theory. Assuming that Eq. 17 can be applied to the spinel layer in the present duplex-oxide layers and the iron activity at oxide/steel interface equals 1, the parabolic growth constant can be calculated using Eq. 30 and $K_p[calculated] = 3.21 \times 10^{-17}\,\mathrm{m^2/s}$. This value is similar to the values for SUS 316 steel calculated from Satio *et al.*[52] and Smith[51] expressions that are $4.75 \times 10^{-18}\,\mathrm{m^2/s}$ and $2.64 \times 10^{-17}\,\mathrm{m^2/s}$, respectively, under the same oxygen partial pressure.

To calculate K_r, detailed experimental conditions such as the test-loop length, the temperature profile, etc. have to be known. However, based on our previous analysis[46] the corrosion rate q is less than 0.01 mm/yr at 550°C when oxygen concentration is around 0.01 ppm. Assuming $q = 0.01$ mm/yr, we obtain $K_r[calculated] = 9.1 \times 10^{-13}$ m/s using Eq. 24. It is noted that the above calculations can not show the steel composition effects on the oxide-layer formation.

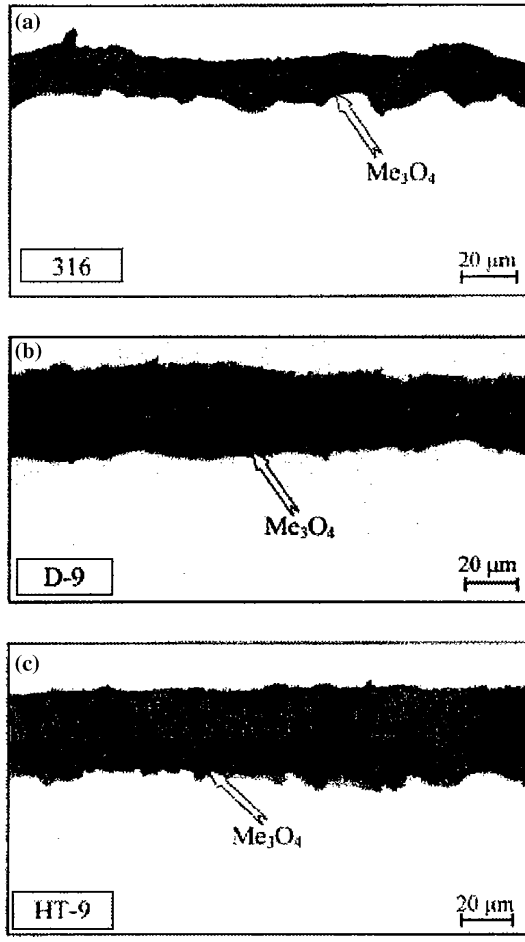

Fig. 12. Duplex-layer-oxide structure for steel (a) D-9, (b) 316 and (c) HT-9 after 2000 h exposures in flowing LBE with a velocity 2 m/s and oxygen concentration in the range of 0.03–0.05 ppm.[17]

There are many uncertainties in the experiments, such as the iron-diffusion coefficient in LBE, the loop-global condition effects, the grain-size effects, etc. making it difficult to obtain exact values of the rate constants theoretically. However, Eqs. 34 and 35 provide simple expressions to fit the experimental results. The fitted results of the weight changes of D-9 and HT-9 steels are shown in Fig. 13. Because there is significant erosion of steel 316 after 1000 h, it is impossible to fit the results using the present model

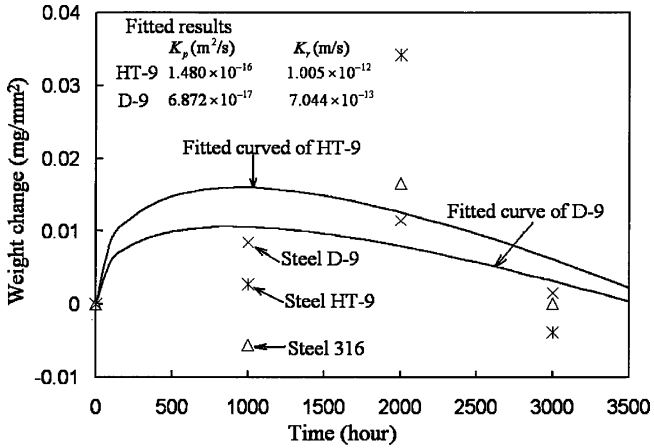

Fig. 13. Fitted results of sample weight changes.

that only considers the mass-transfer corrosion caused scale removal. But experimental results of steel 316 are also shown for comparison. Although the agreement is less than satisfactory, we believe that the key feature is captured and long-term, corrosion test-data are needed for further validation.

The fitted value of the parabolic rate constant, K_p, is $1.480 \times 10^{-16}\,m^2/s$ for HT-9 and $6.872 \times 10^{-17}\,m^2/s$ for D-9. It is reasonable that the K_p of HT-9 is larger than that of D-9 considering D-9 has higher contents of Cr and Ni than HT-9. These fitted values are greater than the calculated value, but the difference is deemed acceptible considering there are many uncertainties.

Although the two samples were put into the same test leg simultaneously and tested under the same condition, the fitted K_r of the two steels have some differences ($1.01 \times 10^{-12}\,m/s$ for HT-9 and 7.04×10^{-13} for D-9) owing to large scatter in the data. Both are however close to the calculated value. According to the present simplified model, the scale removal rate of Fe_3O_4 is dependent only on the flow condition and the temperature and is independent of steel compositions. Study on composition effects on corrosion will need more careful and longer-term experiments.

Using the fitted values of K_p and K_r, comparisons between the calculated results and the experimental results of the duplex-layer-oxide thickness are shown in Fig. 14. The figure indicates that the results agree with each other reasonably well. The calculated limiting-oxide thickness δ_c is roughly $73\,\mu m$ for HT-9 and $49\,\mu m$ for D-9 at the present operating conditions.

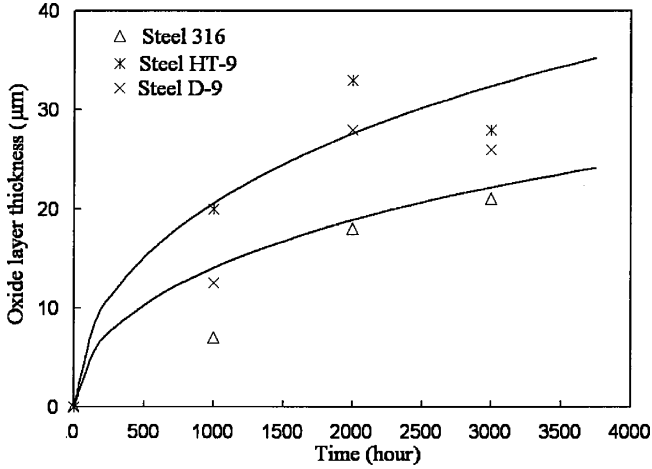

Fig. 14. Comparisons between the theoretical calculation results and experimental results.

CONCLUSIONS

A model for predicting oxide-layer growth and corrosion of steel in liquid lead and lead–bismuth is presented based on Wagner's model for steel oxidation in gaseous environments. The scale is continuously removed by mass-transfer corrosion, which is taken into account through Tedmon's equation. Chemical reactions are assumed to be very fast compared with chemical-mass diffusion and at local equilibria. In the solid phase (oxide layer), outward-iron-ion diffusion controls the oxidation rate. In the liquid phase (liquid lead or liquid lead–bismuth), corrosion-product transport in the mass-transfer boundary layer controls the scale-removal rate.

The oxide structure of steels in liquid–lead alloys is identified based on analyses of the available experimental results. A duplex-layer structure is always formed on martensitic steels at temperatures below 550°C, while for austenitic steels, the oxide layer can have either single-or duplex-layer structure depending on the operation temperature and surface treatments. It is shown that the outer layer (Fe_3O_4) is formed by outward-iron diffusion and the inner layer is due to inward-oxygen diffusion through fast paths. The inner layer takes up the space by outward-iron diffusion. Cr and Ni are relatively enriched in the inner layer which increases the protectiveness over time.

The oxide thickness can reach a limiting thickness that is determined by the ratio of the parabolic-rate constant to the removal-rate constant. For long-term operation, the control step will eventually be diffusion in the

inner layer. The outer layer will dissociate and will be completely removed by mass-transfer corrosion, making Fe–Cr spinel the outer layer. It is also shown that the possibility exists for the formation of a pure-Cr-oxide layer underneath the Fe–Cr spinel by heavy depletion of iron.

Parametric dependencies are discussed. Contrary to Roberson's model for aqueous environments, the present model shows that the instantaneous thickness and the limiting value are very sensitive to the mass-transfer rate in the liquid-mass-transfer-boundary layer even when the control step is in the inner layer. At the steady state, the original-steel-surface-recession rate is determined only by the mass-transfer-corrosion rate, indicating that the oxidation of steel in liquid–lead alloys depends strongly on the flow velocity. Different from the purely parabolic law, the oxide-thickness behavior and the sample weight change depend on the initial conditions. The weight can decrease even for the cases of oxide growth with time.

The present model is partially benchmarked by applying it to interpret the test results of several steels in a LBE loop. It is should be noted that the present study is a very preliminary evaluation of the oxide behaviors of steel in liquid–lead alloys at high temperatures. The oxidation process with scale removal by flowing liquid is a very complex process depending on many factors. To optimize the protective of layer of structure in lead-alloy-coolant system, a complete study of the oxide behaviors should be carried out experimentally and theoretically. However, the key qualitative features are captured in this model and can serve as the starting point for bringing this area of research to the next level.

REFERENCES

1. J. Zhang, and N. Li, *Corrosion* **60**, 331 (2004).
2. G. Ilincev, *Nuclear Engineering and Design* **217**, 167 (2002).
3. B.F. Gromov, *et al.*, *Nuclear Engineering and Design* **173**, 207 (1997).
4. N. Li, *Journal of Nuclear Materials*, **300**, 73 (2002).
5. F. H. Stott, *Reports on Progress in Physics* **50**, 861 (1987).
6. P. Kofstad, *High Temperature Corrosion*, (Elsevier Applied Science Publishers. Ltd. 1987) p. 413.
7. F. Barbier, G Benamati, C. Fazio, and A. Rusanov, *Journal of Nuclear Materials* **295**, 149 (2001).
8. H. Glasbrenner, J. Konys, G Mueller, and A. Rusanov, *Journal of Nuclear Materials* **296**, 237 (2001).
9. F. Balbaud-Celerier, P. Beloffre, A. Terlain, and A. Rusanov, *J. Phys. IV. France* **12**, Pr8-177 (2002).
10. C. Fazio, I. Ricapito, G. Scaddozzo, and G. Benamati, *Journal of Nuclear Materials* **318**, 325 (2003).
11. C. Fazio, G. Benamati, C. Martini, and G. Palombarini, *Journal of Nuclear Materials* **296**, 243 (2001).
12. G. Benamati, C. Fazio, H. Piankova, and A. Rusanov, *Journal of Nuclear Materials* **301**, 23 (2002).
13. G. Muller *et al.*, *Journal of Nuclear Materials* **301**, 40 (2002).

14. L. S. Crespo, F. J. Martin Munoz, and D. G. Briceno, *Journal of Nuclear Materials* **296**, 273 (2001).
15. D. G. Briceno *et al*., *Journal of Nuclear Materials* **303**, 137 (2002).
16. F. Barbier and A. Rusanov, *Journal of Nuclear Materials* **296**, 231 (2001).
17. J. Zhang, N. Li, Y. Chen, and A. Rusanov, *Journal of Nuclear Materials* **336**, 1 (2005).
18. J. Zhang and N. Li, *Report to Los Alamos National Laboratory* 2004, LA-UR-04-0869.
19. C. Wagner, *Corrosion Science* **9**, 91 (1969).
20. C.S. Tedmon Jr, *Journal of Electrochemical Society* **113**, 766 (1966).
21. B. Stellwag, *Corrosion Science* **40**, 337 (1998).
22. J. E. Castle and H. G. Masterson, *Corrosion Science* **6**, 93 (1966).
23. R. Winkler, F. Huttner, and F. Michel, *VGB Kraftwerkstechnik* **69**, 527 (1989).
24. D.H. Lister, R.D. Davidson, and E. McAlpine, *Corrosion Science* **27** 113 (1987).
25. J. Robertson, *Corrosion Science* **29**, 1275 (1989).
26. A. Atkinson, *Reviews of Modern Physics* **57** (2), 437 (1985).
27. G. B. Gibbs, *Oxidation of Metals* **7**, 173 (1973).
28. R. J. Hussey and M. J. Graham, *Corrosion Science* **21**, 255 (1981).
29. J. Robertson, *Corrosion Science* **32**, 443 (1991).
30. F. Balbaud-Celerier, A. Terlain, P. Fauvet, and C. Richet, "Corrosion of Steels in Liquid Lead Alloys Protected by an Oxide layer Application to the MEGAPIE target and to the Russian Reactor Concept BREST 300", *Report Technique RT-SCCME 630*, CEA Report (2003).
31. A. Atkinson, *Corrosion Science* **22**, 87 (1982).
32. C. Wagner, *Corrosion Science* **8**, 889 (1969).
33. C. Wagner, *Progress in Solid State Chemistry* **10**, 3 (1976).
34. F. Gesmundo, *Materials Science and Engineering* **87**, 243 (1987).
35. N. J. Cory and T. M. Herrington, *Oxidation of Metals* **28**, 237 (1987).
36. W. W. Smeltzer, R. R. Haering, and J. S. Kirkaldy, *ACTA Metallurgica* **9**, 880 (1961).
37. A. Atkinson, R. I. Taylor, and A. E. Hughes, *Philosophical Magazine A* **45**, 823 (1982).
38. R. Dieckmann and H. Schmalzried, *Berichte der Bunsen-Gesellschaft-Physical Chemistry Chemical Physics* **81**, 344 (1977).
39. R. Dieckmann and H. Schmalzried, *Berichte der Bunsen-Gesellschaft-Physical Chemistry Chemical Physics* **81**, 414 (1977).
40. R. Dieckmann and H. Schmalzried, *Berichte der Bunsen-Gesellschaft-Physical Chemistry Chemical Physics* **82** 778 (1978).
41. N. L. Peterson, W. K. Chen, and D. Wolf, *J. Phys. Chem. Solids*., **41**, 709 (1980).
42. P. Kofstad, *High Temperature Corrosion*, (Elsevier Applied Science Publishers Ltd. 1987) p. 44.
43. J. Topfer, S. Aggarwal, and R. Dieckmann, *Solid State Ionics* **81**, 251 (1995).
44. A. Atkinson, M. L. Odwyer, and T. I. Taylor, *Journal of Materials Science* **18**, 2371 (1983).
45. J. Zhang and N. Li, *Nuclear Technology* **144**, 379 (2003).
46. J. Zhang and N. Li, *Journal of Nuclear Materials* **321**, 184 (2003).
47. F. Balbaud-Celerier and F. Barbier, *Journal of Nuclear Materials* **289**, 227 (2001).
48. J. Zhang and N. Li, *Journal of Nuclear Materials* (in press 2005).
49. H. Schmalzried, *Zeitschrift fur Physikalische Chemie Neue Folg* **31**, 184 (1962).
50. P. Surman, *Corrosion Science* **13**, 825 (1973).
51. A. F. Smith, *Corrosion Science* **22**, 857 (1982).
52. M. Saito, H. Furuya, and M. Sugisaki, *Journal of Nuclear Materials* **135**, 11 (1985).
53. A. F. Smith, *Corrosion Science* **21**, 529 (1981).
54. H. Furuya, M. Satito, and M. Sugisaki, *Journal of Nuclear Materials* **154**, 128 (1988).
55. S. L. Chang, F. S. Pettit, and N. Birks, *Oxidation of Metals* **34**, 71(1990).
56. D. M. Rishel, F. S. Pettit, and N. Birks, *Materials Science and Engineering*, A **143**, 197 (1991).
57. H. Taimatsu, *Journal of the Electrochemical Society* **146**, 3686 (1999).